[ISSN 0911-5501]

NRO

Nobeyama
Radio
Observatory
Report
No. 550
2001

VLBI Monitoring Observations of Water Masers Around the Semi-Regular Variable Star R Crateris

José K. ISHITSUKA, H. IMAI, T. OMODAKA, M. UENO, O. KAMEYA,
T. SASAO, M. MORIMOTO, T. MIYAJI, J.-I. NAKAJIMA,
and T. WATANABE

NOBEYAMA RADIO OBSERVATORY OF THE NATIONAL ASTRONOMICAL OBSERVATORY
NOBEYAMA, MINAMISAKU, NAGANO-KEN 384-1305, JAPAN

VLBI Monitoring Observations of Water Masers Around the Semi-Regular Variable Star R Crateris

José K. Ishitsuka ,[1] Hiroshi Imai,[2,3] Toshihiro Omodaka,[4] Munetaka Ueno,[1]
Osamu Kameya,[2,3] Tetsuo Sasao,[3] Masaki Morimoto,[5]
Takeshi Miyaji,[3,6] Jun-ichi Nakajima,[7] and Teruhiko Watanabe[4]

[1]*Department of Earth Science and Astronomy, University of Tokyo, Komaba, Tokyo 153-8902*
pepe@chianti.c.u-tokyo.ac.jp

[2]*Mizusawa Astrogeodynamics Observatory, National Astronomical Observatory, Mizusawa, Iwate 023-0861*

[3]*VERA Project Office, National Astronomical Observatory, Mitaka, Tokyo 181-8588*

[4]*Faculty of Science, Kagoshima University, Kagoshima, Kagoshima 890-0065*

[5]*Nishi-Harima Astronomical Observatory, Sayo, Hyogo 679-5313*

[6]*Nobeyama Radio Observatory, National Astronomical Observatory, Minamisaku, Nagano 384-1305*

[7]*Kashima Space Research Center, Communications Research Laboratory, Kashima, Ibaraki 314-0012*

(Received 2000 December 8; accepted 2001 September 24)

Abstract

We monitored water-vapor masers around the semi-regular variable star R Crateris with the Japanese VLBI Network (J-Net) at the 22 GHz band during four epochs with intervals of one month. The relative proper motions and Doppler-velocity drifts of twelve maser features were measured. Most of them existed for longer than 80 days. The 3-D kinematics of the features indicates a bipolar expanding flow. The major axis of the asymmetric flow was estimated to be at P.A. = 136°. The existence of a bipolar outflow suggests that a Mira variable star had already formed a bipolar outflow. The water masers are in a region of apparent minimum radii of 1.3×10^{12} m and maximum radii of 2.6×10^{12} m, between which the expansion velocity ranges from 4.3 to 7.4 km s^{-1}. These values suggest that the water masers are radially accelerated, but still gravitationally bound, in the water-maser region. The most positive and negative velocity-drifting features were found relatively close to the systemic velocity of the star. We found that the blue-shifted features are apparently accelerated and the red-shifted apparently decelerated. The acceleration of only the blue-shifted features seems to be consistent with that of the expanding flow from the star.

Key words: masers — stars: late-type — stars: individual (R Crateris)

1. Introduction

The gas dynamics of circumstellar envelopes (CSEs) during the latest phase of the asymptotic giant branch (AGB) stars is one matter of debate to elucidate the physical mechanisms of energetic mass loss of evolved stars. The AGB stars evolve in a sequence of Mira variables, IRC (or AFGL) objects, OH/IR stars, proto-planetary nebulae (PPNs), and planetary nebulae (PNs) (Takaba et al. 1994). Recent HST infrared images (e.g. Sahai et al. 1998) have shown asymmetric or bipolar outflows around the central object of PNs; PNs show axisymmetric morphologies in over 50% of the cases (e.g. Sahai et al. 1998; Manchado et al. 2000). On the other hand, the CSEs of AGB stars are generally spherically symmetric (Manchado et al. 2000). The most intriguing question is when the change of morphology occurs between the AGB and PN phases.

Water-vapor masers have been well observed around many evolved stars. A cluster of water-maser features exists at $10^{12} - 10^{13}$ m from the central star (Johnston et al. 1985; Lane et al. 1987). Maser action is predicted in the inner part of the CSE, and the size of the maser region increases with the stellar mass-loss rate (Cooke, Elitzur 1985). Distributions of water masers in CSEs are complex, and change with time (e.g. Lane 1982; Johnston et al. 1985). The time variation was reported on a scale ranging from a few weeks to a few years (Bowers et al. 1989). The VLA, VLBA, and MERLIN observations have monitored the water-maser features: the epochs were widely scattered from a half year to several years (Marvel 1996). Measurements of the relative proper motion of compact maser features with high spatial resolution can be used to investigate the structure of CSEs and to trace those asymmetries or bipolarities (Marvel 1996). Measurements of 3-D velocities of water-maser features as well as their radial-velocity drifts (Imai et al. 1997) enable us to elucidate the dynamics of the mass-loss process in more detail. For this purpose, monitoring observations within intervals of a few weeks are necessary to verify whether the same maser features are observed within the epochs.

R Crt is a semi-regular variable star of SRb type in spectral classification M7 (Kholopov et al. 1987). R Crt is classified as a Mira variable from a color-color diagram of *IRAS* observations (Takaba et al. 1994). The V-band magnitude varies between 9.8 and 11.2 mag with a pulsation period of 160 days. ^{12}CO(J=2−1) and (J=1−0) and ^{13}CO(J=2−1)(Kahane, Jura 1994) as well as OH and SiO masers (Le Squeren et al. 1979; Jewell et al. 1991) were detected at the envelope. The mass-loss rate of R Crt was estimated to be $1.0 \times 10^{-6}\ M_{\odot}\ \mathrm{yr}^{-1}$ (Kahane, Jura 1994) from CO observation. The systemic velocity for R Crt is 10.8 km s^{-1} (Bowers 1992), which was estimated from the center velocity of the velocity coverage of a CO observation profile. Water masers around R Crt were first detected by Dickinson et al. (1973). In this paper we present the results of monitoring observations for water masers around R Crt. We compared the positions of the water-maser features among epochs separated by a few weeks, and measured radial velocities throughout the epochs. Based on the 3-D motions and

Table 1. J-Net telescopes that participated in the observations.

Station	Designation	Diameter (m)	Ap. efficiency (%)	T_{sys} at zenith (K)
Mizusawa	M	10	36	140 – 330
Kashima	O	34	57	280 – 340
Nobeyama	N	45	63	240 – 290
Kagoshima	K	6	40	170 – 220

radial-velocity drifts, we discuss the dynamics of the mass-loss flow from this star.

2. Observations and Data Reduction

Monitoring observations of R Crt at R.A. (B1950.0) = $10^{\rm h}58^{\rm m}6\overset{\rm s}{.}14$ and Decl. (B1950.0) = $-18°03'18\overset{''}{.}27$ were made by using the Japanese VLBI Network (J-Net, Omodaka et al. 1994) from 1998 March to June, at four epochs with an interval of a few weeks. J-Net is comprised of three of the National Astronomical Observatory of Japan's telescopes, including the 45-m telescope at Nobeyama Radio Observatory (*), the 10-m telescope at Mizusawa, and the 6-m telescope at Kagoshima, as well as one of the Communications Research Laboratory's telescopes, the 34-m telescope at Kashima. Table 1 gives the characteristics of the telescopes, and table 2 the observations.

In each epoch R Crt was observed at 5 to 8 intervals for 20 to 40 minutes alternating a scan for 5 to 10 minutes toward 3C 273B as a calibrator. The observed signals were recorded with the VSOP terminal (Kawaguchi et al. 1994) in one base band channel with a band width of 16 MHz in 2 bits per sample. The recorded data were correlated using the Mitaka FX Correlator (Chikada et al. 1991). The output of the correlator had an 8 MHz bandwidth with 512 spectral channels, corresponding to a Doppler velocity resolution of 0.105 km s^{-1}. The velocity coverage was from $V_{\rm LSR} = -16$ km s^{-1} to 36 km s^{-1} centered on the water-maser line.

We used the NRAO's AIPS software to calibrate, image and fit the brightness distribution. The strongest water maser component detected at $V_{\rm LSR} = 15.03$ km s^{-1} was used as phase reference in each set of observations. The synthesized beam of the array was 8 mas × 3 mas with a position angle of − 40° in natural weight. The typical rms thermal noise level in the channel maps ranged from 34 mJy to 80 mJy between the first and last epochs (see table 2). The accuracy of the intensity scale is estimated to be better than 50%. The accuracy of the relative angular position ranged from 0.2 mas to 0.9 mas in the R.A. direction and 0.2 mas to 1.1 mas in the declination direction, in a single velocity channel.

(*) Nobeyama Radio Observatory is a branch of the National Astronomical Observatory, operated by the Ministry of Education, Culture, Sports, Science, and Technology(, Japan).

Table 2. Time table of the monitoring observation.

Experiment name	Epoch (1998)	Stations	Observation duration (hr)	Typical rms thermal noise (mJy)	Number of detected features
j98090	March 31	MKNO	10	34	14
j98116	April 26	MKNO	10	55	13
j98148	May 28	MKNO	9	70	12
j98170	June 19	MKNO	8	80	5

A maser spot is a single-velocity component, while a maser feature is a group of maser spots within several mas in positions and $0.1 - 0.5$ km s^{-1} in velocities. The definitions of 'maser spot' and 'feature' used in this paper are the same as those used in Imai et al. (2000) and references therein. These definitions are the same as those given by Gwinn (1994). The positions of the brightness peaks in the maser spots were estimated using the AIPS task JMFIT. We traced the position and velocity at the brightness peak in each of the features. We determined the velocity at the brightness peak of a feature by quadratic fitting of the observed intensities against the velocities of the strongest three maser spots in the feature. The position of the feature at the calculated peak velocity was estimated on the line-connecting positions of two velocity-adjacent spots assuming a constant velocity gradient between the two spots.

3. Results and Discussion

For proper-motion measurements, the four maps were superposed so as to situate the position-reference feature ($V_{\rm LSR} = 15.03$ km s^{-1}) at the same position in the superposed single map. Figure 1 shows the observed proper motions of the maser features in the R.A. and Decl. directions. We also measured the Doppler-velocity drifts of the maser features that are shown in figure 1. The uncertainty of the relative velocities of the maser features was assumed to be 0.05 km s^{-1}, one half of our velocity resolution. Since the position-reference is also moving relatively, the mean proper motion of the features was calculated and subtracted from each of the proper motions. Table 3 summarizes the relative positions, proper motions, Doppler velocities, Doppler-velocity drifts, and peak intensities of the maser features. A letter is assigned to each of the features, and hereafter we use these assignations. We confirmed that the strongest features (D, H, and K) were detected at four epochs, and existed for at least 80 days, while others were detected during two or three epochs, possibly due to noisy observation at the third and fourth epoch.

Figure 2 shows the obtained 3-D motions of the water-maser features. A clear separation between the blue-shifted and red-shifted maser features was found in the southeast and northwest directions, which indicate bipolar outflow. The former side of the outflow has a velocity of -8.68 km s^{-1} with respect to the systemic velocity, while the latter has a velocity of 5.45 km

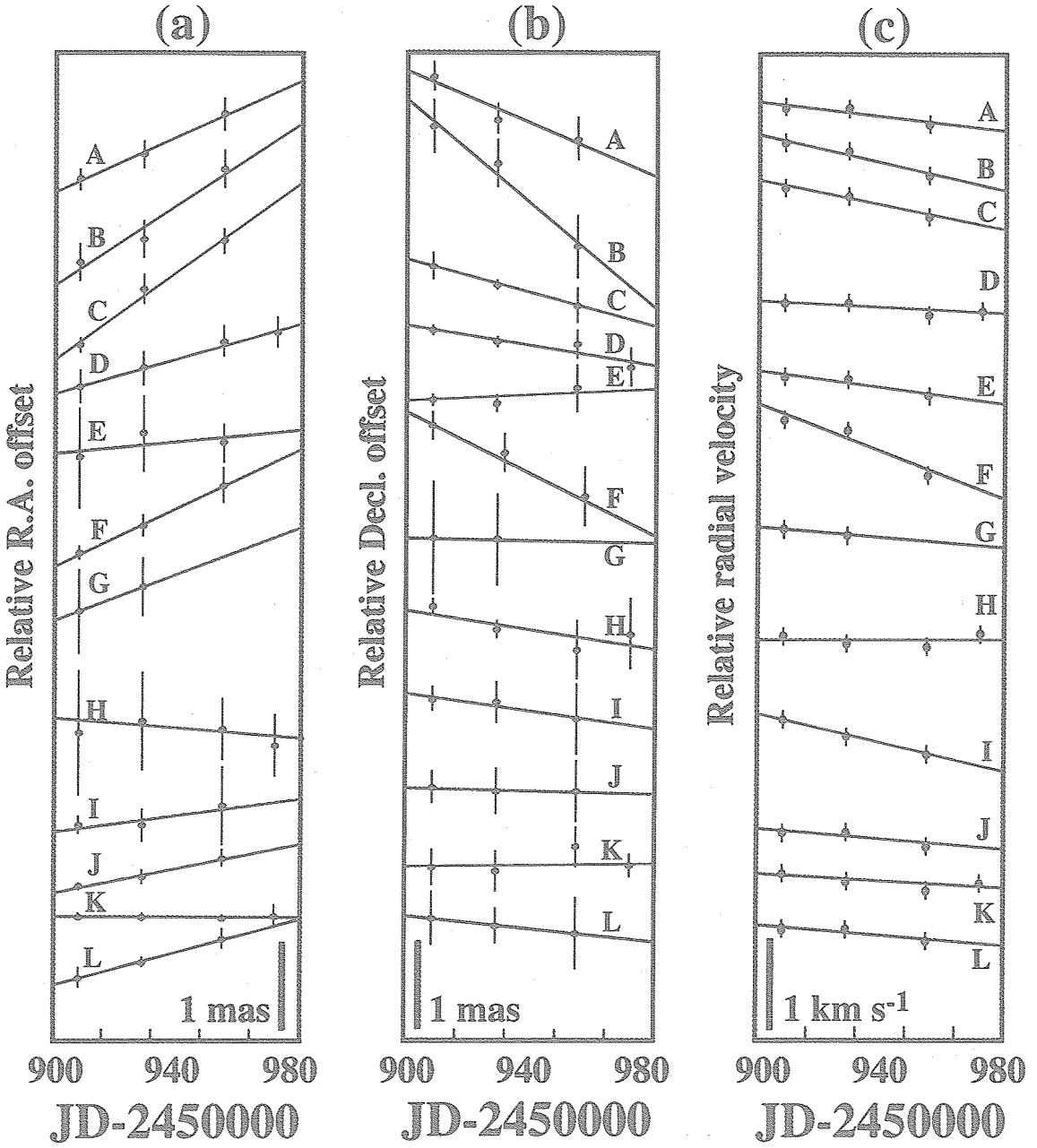

Fig. 1. Time variation of R Crt maser features in (a) R.A., (b) Decl., and (c) the Doppler velocity. Features A – G are blue-shifted features and H – L red-shifted features, with respect to the systemic velocity, $V_{\rm LSR} = 10.8$ km s^{-1}.

Table 3. Obtained parameters of the water-maser features with proper motions.

	Position		Relative velocity				V_z drift		Peak intensity			
Feature	ΔX	ΔY	μ_x	σ_{μ_X}	μ_y	σ_{μ_Y}	$V_z{}^*$	ΔV_Z	$\dot{V}_z$	$\sigma_{\dot{V}_z}$	Epoch 1	Epoch 2	Epoch 3	Epoch 4
	(mas)	(mas)	(km s^{-1})		(km s^{-1})		(km s^{-1})		(km s^{-1}yr^{-1})		(Jy beam^{-1})			
A	48.23	−68.58	2.55	2.35	−4.00	3.59	−7.44	0.73	−1.37	0.45	7.87	3.07	1.43	...
B	46.20	−64.82	0.84	7.45	−6.34	11.11	−6.88	0.42	−1.27	0.99	5.48	1.62	...	...
C	65.52	−3.05	7.66	1.80	−2.38	3.06	−5.41	1.09	−2.30	0.45	2.09	6.32	1.92	...
D	−47.03	36.59	−0.25	2.19	0.93	1.36	−1.81	0.76	−0.68	0.30	1.45	5.61	2.32	2.31
E	−55.34	42.34	−4.64	5.87	4.11	2.52	−0.71	0.99	−1.55	0.45	3.64	1.33	1.47	...
F	53.42	−37.67	2.84	2.07	−6.2	4.23	−0.24	1.58	−4.32	0.45	2.62	1.43	0.86	...
G	−62.24	40.48	3.68	19.10	4.78	11.30	0.42	0.36	−0.98	0.99	2.18	0.73	...	...
H	−67.80	38.97	−7.96	7.02	0.33	1.30	1.12	0.95	0.05	0.30	8.93	3.91	2.18	2.97
I	−72.40	38.78	0.67	13.00	−0.97	5.08	1.91	0.73	−2.52	0.81	2.19	1.41	0.64	...
J	20.09	46.81	−0.62	2.08	2.95	2.12	2.72	0.81	−1.04	0.45	1.76	1.29	1.16	...
K† ...	0.00	0.00	−5.54	0.59	4.46	0.95	4.23	1.21	−0.73	0.30	30.40	30.07	25.20	20.35
L	−0.46	46.02	0.77	1.37	2.32	2.58	6.56	1.09	−1.04	0.45	8.98	2.17	0.90	...

* Relative Doppler velocity with respect to the systemic velocity $V_{\rm LSR}$ = 10.80 km s^{-1}

† Position reference feature at $V_{\rm LSR}$ = 15.03 km s^{-1}

s^{-1}. Features A, B, C, and F are within the blue-shifted side of the outflow, and spots G, H, and I are within the red-shifted side of the suggested bipolar outflow. Spots D and E possibly belong to the red-shifted side of the outflow, but have blue-shifted motions.

3.1. Objective Analysis with VVCM

To quantify the suggested bipolarity noted from figure 2, we used the VVCM (Variance-covariance matrix) technique, which fully and objectively extracts the kinematic essentials, without assuming any particular model (Bloemhof 2000). The elements of the VVCM matrix are expressed as

$$\sigma_{ij} = \frac{1}{N-1}\sum_{n=1}^{N}(v_{i,n}-\overline{v}_i)(v_{j,n}-\overline{v}_j), \tag{1}$$

where the diagonal elements are the velocity dispersions. Here, i and j denote the three orthogonal space axes (R.A., Decl., and radial coordinates z), n is the n-th maser feature of the total N features, and the bar indicates the average over maser features. The VVCM matrix and the respective diagonalization for R Crt were obtained as follows (in units of km^2 s^{-2}):

$$\begin{pmatrix} 18.55 & -7.35 & -8.10 \\ -7.35 & 15.97 & 11.43 \\ -8.10 & 11.43 & 18.79 \end{pmatrix} \Rightarrow \begin{pmatrix} 35.82 & 0 & 0 \\ 0 & 11.62 & 0 \\ 0 & 0 & 5.86 \end{pmatrix}. \tag{2}$$

In figure 2, the two bold vectors show two-dimensional projections of two unit eigenvectors with the largest eigenvalues of the VVCM diagonalization. The eigenvector $\mathbb{V}_1$ with the

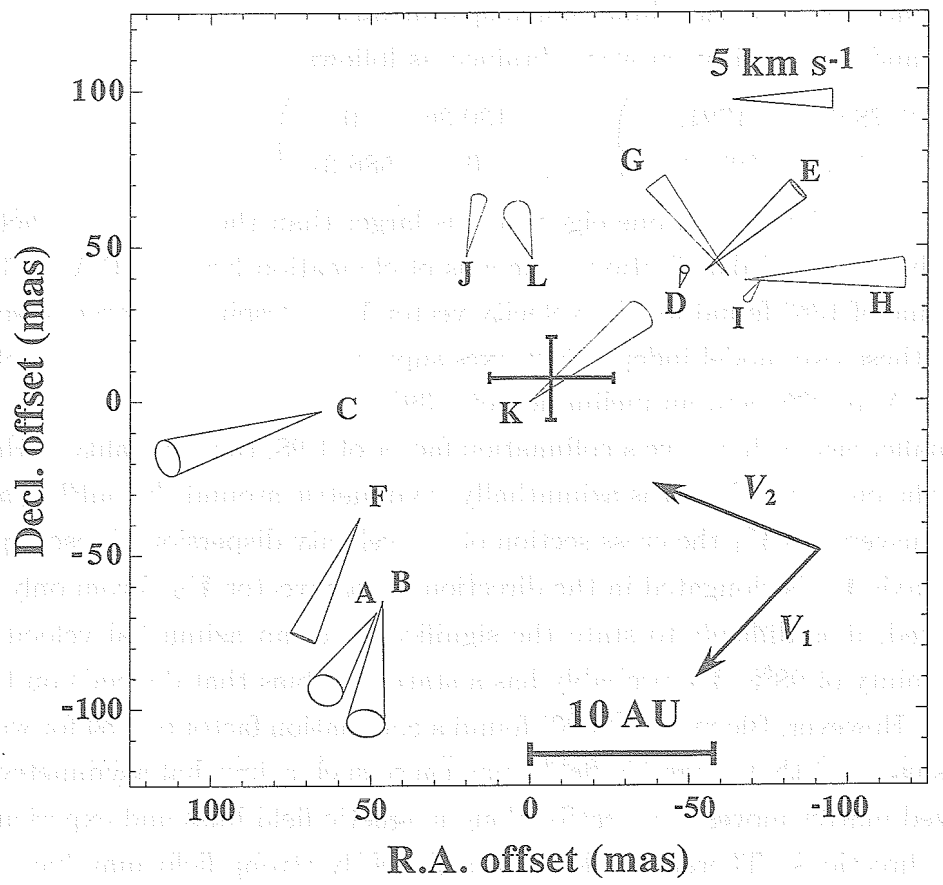

Fig. 2. 3-D motions of maser features represented in scaled cones. The maser features are at the apex of the cones. The red and blue cones show red- and blue-shifted features, with respect to the systemic velocity. The inclination of the cone indicates the degree of the Doppler velocity with respect to the transverse velocity. The big plus-sign at the center is the model-calculated position of R Crt; the size of the plus-sign shows the positional uncertainties. The bold arrows are eigenvectors: $\boldsymbol{V_1}$, the largest eigenvector (the VVCM outflow axis) and $\boldsymbol{V_2}$, the second-largest eigenvector.

largest eigenvalue, V_1= 35.82 km^2 s^{-2}, is the major principal axis of the VVCM; the direction of the axis corresponds to the outflow axis. The axis of $\boldsymbol{V_1}$ lies at a P.A. of 136°, and is inclined at an angle of −39° with respect to the plane of the sky with the southeast lobe directed out of the page (towards the observer). The second-largest eigenvector $\boldsymbol{V_2}$, with the second-largest eigenvalue, V_2= 11.62 km^2 s^{-2}, is at P.A. of 68° east of north, and is inclined at an angle of 24° with respect to the plane of the sky; the vector is directed into the plane. The collimation factor between the two largest eigenvalues, V_1 and V_2, is 3.08, and 1.98 between the smallest, V_2 and V_3. On the other hand, a Monte Carlo simulation gave the following values: V_1= 70.6 ± 52.9 at P.A. 66°.5 ± 64°.9, an inclination of −4°.5 ± 23°.6, V_2= 24.2 ± 11.5 at P.A. 34°.2 ± 59°.3 and an inclination of 26°.8 ± 25°.4. This simulation gave the following values of the collimation factors: 3.1 ± 1.9 for V_1, V_2 and 3.2 ± 1.8 for V_2, V_3.

We also analyzed the two-dimensional spatial variance-covariance matrix (SVCM). The SVCM matrix and diagonalization were obtained as follows:

$$\begin{pmatrix} 2778.91 & -1721.37 \\ -1721.37 & 1937.82 \end{pmatrix} \Rightarrow \begin{pmatrix} 4130.36 & 0 \\ 0 & 586.37 \end{pmatrix}. \quad (3)$$

Diagonalizing the matrix, one eigenvalue is larger than the other by a factor of 7, indicating a slightly elongated distribution. The axis of elongation lies at a P.A. of 128°, which is close to the value of 136° found for the velocity vector V_1. Despite the large uncertainties, the coincidence of these two model-independent axes supports the existence of a bipolar outflow of R Crt with a P.A. of 136° and an inclination of −39°.

The smaller eigenvalues give a collimation factor of 1.98, the inequality of the eigenvalues suggests that the outflow of R Crt is azimuthally asymmetric around the outflow axis V_1. This means that transverse to V_1 the cross section of the velocity dispersion ellipsoid perpendicular to the outflow axis V_1 is elongated in the direction of eigenvector V_2. From only the 12 maser features detected, it is difficult to state the significance of an azimuthal velocity asymmetry with an uncertainty of 98%. V_2 probably has a statistical bias that depends on the number of maser features. However, Bloemhof (2000) found a collimation factor of 1.54 for water masers in W 49N, and suggested that magnetic fields may cause such azimuthal asymmetry. Due to flux freezing, ionized matter moves most easily along magnetic field lines and experiences magnetic drag in other directions. Therefore, flow in a sufficiently strong field may have an elongated cross section in velocity space, and V_2 may indicate the direction of elongation. Szymczak et al. (1999) measured magnetic fields by observing linearly polarized OH 1667 MHz masers of R Crt in 1995. The results indicate that the magnetic field subtends a position angle of −30°, almost parallel to vector V_1. This may be a coincidence, since the magnetic field observation lasted for $\sim$ 3 years before our observations. Therefore, we need simultaneous observations of a magnetic field and maser proper motions in order to confirm the correlation between the magnetic fields and eigenvector V_1.

3.2. Constructing the 3-D Kinematical Model

In order to derive kinematic parameters of the CSE around R Crt, the 3-D motions of the features were fitted to an expanding outflow model. First, the 3-D model assumes an expanding outflow where the velocity vectors depart radially from a common center. The details of the fitting were described by Imai et al. (2000). We estimated only the position and the systemic motion of the star as free parameters, but assumed the values of the distance to be $d = 170$ pc and the stellar velocity to be 10.8 km s^{-1}. Table 4 summarizes the estimated parameters in the model fitting. Second, the expansion velocity was estimated by fitting the data to the 2-D standard expansion model. This model traces an ellipse on a radius-$V_{\rm LSR}$ plot, and provides a reasonable description of the water maser CSE. In the case of the standard expanding outflow model, the projected radius, r, of the maser feature at a velocity $V - V_0$ is given by

Table 4. Best-fit model for the maser velocity field for R Crt.

Parameter	Offset
Velocity:	
V_{0x}* (km s^{-1})	5.4±3.9
V_{0y}* (km s^{-1})	−5.7±3.9
V_{0z}† (km s^{-1})	10.8
Position:	
x_0* (mas)	−9±21
y_0* (mas)	10±13
RMS residual $\sqrt{S^2}$	0.47

* Relative value with respect to the position-reference maser feature.
† Assuming the systemic velocity: $V_{0z} = 10.8$ km s^{-1}.

$$r = r_0 \left[1 - [(V - V_0)/V_{\rm exp}]^2\right]^{1/2}, \tag{4}$$

where V_0 is the systemic velocity of the star, r_0 the CSE radius, and $V_{\rm exp}$ the expansion velocity at the CSE. Figure 3 shows a radius-$V_{\rm LSR}$ plot for R Crt and modeled ellipses. Least-squares fits of equation (4) using the data (A − L features) gave average values of $V_{\rm exp} = 7.4$ km s^{-1} and a CSE radius corresponding to $r_0 = 2.6 \times 10^{12}$ m. The inner envelope fits to the parameters of $r_i = 1.3 \times 10^{12}$ m and $V_{\rm exp} = 4.3$ km s^{-1}. Colomer et al. (2000) estimated the radius of the water maser envelope of R Crt using the VLA as 2.1×10^{12} m with $V_{\rm exp} = 8$ km s^{-1} at an assumed distance of 170 pc, which is consistent with our estimate with compact and bright features (c.f. Bowers, Johnston 1994). The inner radius of the water-maser envelope emission is slightly larger than the typical radius of a dust shell with infrared emission (Danchi et al. 1994). Thus, maser features are likely to lie just above the dust shell where maser clouds are accelerated by radiative pressure (Danchi et al. 1994 and references therein). The inner radius corresponds to a few stellar radii. The radius of the OH emission estimated using the MERLIN array (Szymczak et al. 1999) is 3.6×10^{12} m, where $V_{\rm exp} = 7.9$ km s^{-1}. Szymczak et al. (1999) remarked that this OH envelope should be one of the smallest. Material in the CSE of R Crt is accelerated to reach a terminal velocity of $V = 11.0$ km s^{-1} (Zuckerman, Dyck 1986), which was estimated from CO observations at a maximum radius of 3.1×10^{14} m (Kahane, Jura 1994) at our assumed distance. Thus, the expansion velocity increases with distance. Note, however, that each of the different observations were performed at different epochs.

The strength of the acceleration can be evaluated by comparing the observed expansion velocity, $V_{\rm exp}$, with the escape velocity, $V_{\rm esc}$, given by

$$V_{\rm esc} = \sqrt{\frac{2GM_*}{r_0}}, \tag{5}$$

where G is the gravitational constant and M_* the mass of the star. Assuming a mass of R Crt of 1 $M_\odot$, at the inner radius ($r_i = 1.3 \times 10^{12}$ m, $V_{\rm esc} = 14$ km s^{-1}, $V_{\rm exp} = 4.3$ km s^{-1}), $V_{\rm exp}$ is less than $V_{\rm esc}$; consequently, masers in the inner envelope are gravitationally bound to the

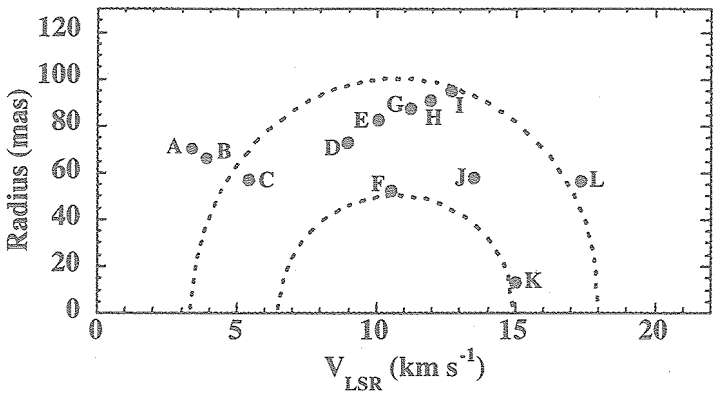

Fig. 3. Model fits assuming a standard expanding outflow. The radius of the outer edge of the water maser region is 100 mas, where the expansion velocity is 7.4 km s^{-1}. The radius of the inner edge is 50 mas, where the expansion velocity is 4.3 km s^{-1}.

star. At the outer radius ($r_0 = 2.6 \times 10^{12}$m, $V_{\rm esc} = 10$ km s^{-1}, $V_{\rm exp} = 7.4$ km s^{-1}), masers are marginally gravitationally bound. Analyses of the velocity fields of supergiants (e.g. VY CMa, S Per, and NML Cyg) suggest that material is, in general, bound to the star at the inner boundary, but unbound at the outer boundary (Yates, Cohen 1994; Richards et al. 1996). The strength of the acceleration in the case of R Crt may be less than those of supergiants.

Finally, we discuss some relationships between the accelerations in the maser regions, the mass-loss rates of the central stars, and the asymmetry of the CSEs. The acceleration is parametrized by the logarithmic velocity gradient, $\epsilon = d(\ln v)/d(\ln r)$ (Richards et al. 1996). For R Crt, within the outer limit of $r = 100$ mas and the inner limit of $r = 50$ mas, the logarithmic velocity gradient is $\epsilon = 0.78$. Table 5 summarizes the velocity gradients, the mass-loss rates, and the asymmetry of the CSEs in R Crt and in some AGB stars. Table 5 shows that the asymmetry of CSEs seems to occur in stars with low velocity gradients ($\epsilon < 0.8$, ex., X Her, R Crt, NML Cyg, and VX Sgr), but not to occur in those with high velocity gradients ($\epsilon > 1.2$, ex., RT Vir and S Per). A large number of samples would clarify this correlation.

3.3. Doppler Velocity Drifts

One of the aims of this work is to measure the Doppler-velocity drifts of individual water-maser features. We found Doppler velocity drifts in the range from $\dot{V}_z = -4.32$ km s^{-1} yr^{-1} (for feature F) to $\dot{V}_z = 0.05$ km s^{-1} yr^{-1} (for feature H). Figure 1 and table 3 indicate that the blue-shifted maser features are apparently accelerated and the red-shifted decelerated. If the blue-shifted maser feature drifts imply true acceleration motions, the blue-shifted side of the outflow would be accelerated towards the terminal velocity, but the red-shifted features would not be accelerated. Analyses of the velocity gradients and the escape velocities suggest that water masers are accelerated in the envelope. It is expected that the red-shifted masers

Table 5. AGB stars mass-loss rates and velocity gradients at the water-maser regions.

Source name	Type	Mass-loss rate † $10^{-6}\ M_\odot\ \mathrm{yr}^{-1}$	Velocity gradient ‡ ϵ	Morphology §
X Her ...	Semi-regular	0.2 (1)	-- (5)	Bipolar (1)
R Crt ...	Semi-regular	1.0 (2)	0.78 (6)	Bipolar (6)
RT Vir ..	Semi-regular	3.0 (3)	3.50 (7)*	Spherical (10)
IK Tau ..	Mira	6.0 (3)	0.84 (7)*	Spherical (11)
S Per	Supergiant	27.0 (3)	1.20 (7)	Spherical (12)
VY CMa	Supergiant	100.0 (3)	0.55 (7)	Ellipsoidal (13)
NML Cyg	Supergiant	180.0 (3)	0.30 (8)	Bipolar (8)
VX Sgr ..	Supergiant	270.0 (4)	0.50 (9)	Bipolar (9)

* Upper limits.

† Mass-loss rates: (1) Kahane, Jura (1996), (2) Kahane, Jura (1994), (3) Yates, Cohen (1994) and references therein, (4) Engels et al. (1983).

‡ Velocity gradients: (5) not available, (6) this work, (7) Yates, Cohen (1994), (8) Richards et al. (1996), (9) Chapman, Cohen (1986).

§ Morphology: (10) Imai H. private communications, (11) Bowers et al. (1993), (12) Richards et al. (1999), (13) Richards et al. (1998)

are decelerated if the driving source of the acceleration does not affect the red-shifted masers at the outer limit of the water-maser envelope.

Remarkable velocity drifts were found for features F, the most negative-drifted, and feature H, the most positive-drifted, F being blue-shifted, and H red-shifted with respect to the systemic velocity at $V_{\mathrm{LSR}} = 10.8$ km s^{-1}. Since features F and H are near the systemic velocity, they move together with the star on the plane of the sky. Features F and H also have a relatively large proper motion on the celestial plane, F having 6.8 km s^{-1} and H having 8.0 km s^{-1} at the assumed distance. On the plane of the sky, features F and H are diagonally separated by $\sim$ 100 mas, and the assumed stellar position lies almost at the center of the diagonal line between the two features. This line between features F and H coincidentally lies at P.A. $\sim$ 136°, which is almost parallel to the VVCM major axis. It is thought that different features do not switch on and off in a small area within the epochs of the observations, because of the simple structure of the maser features. We cannot reject the possibility that the drifts do not reflect the real motions of the circumstellar material.

3.4. Distance to R Crt

The distance to R Crt has been ambiguous, between 300 pc (Knapp et al. 1998) and 170 pc (Szymczak, Le Squeren 1999). For semi-regular variable stars, their intrinsic luminosity

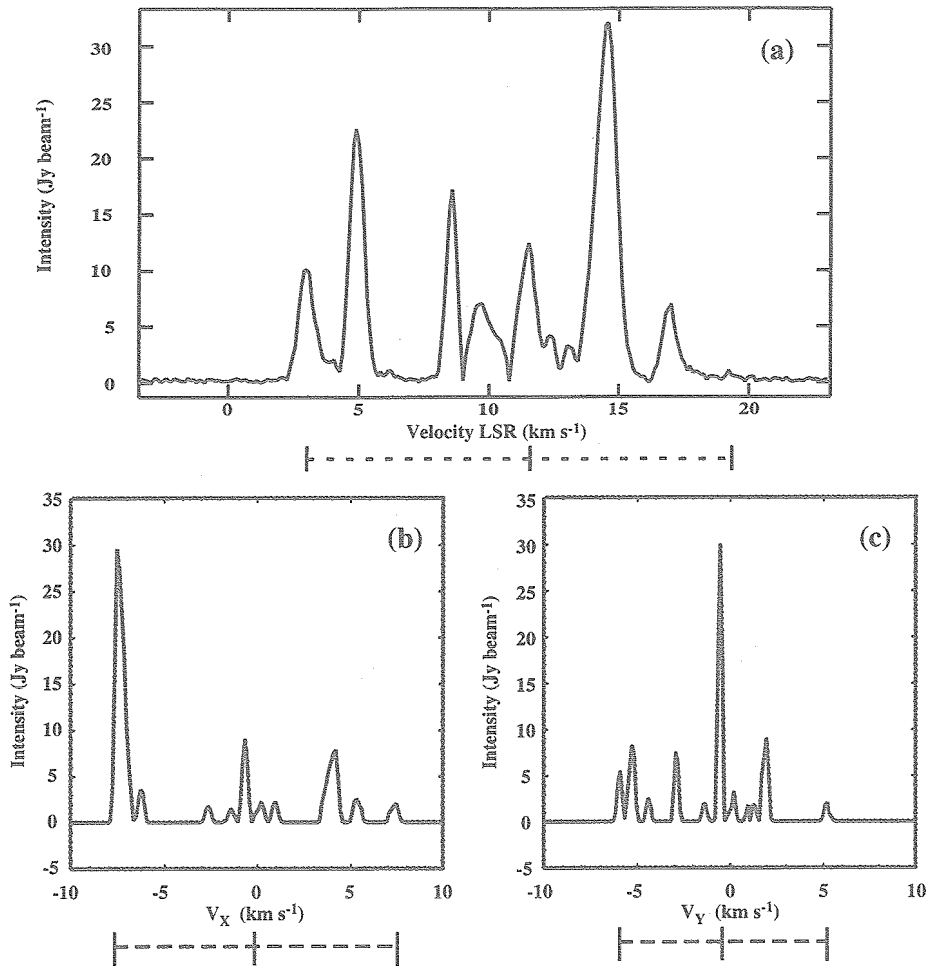

Fig. 4. Spectrum profiles of water masers around R Crt. (a) Total-power spectrum obtained at the first epoch, j98090. Spectrum-like profiles derived from proper-motion measurements, (b) on the P.A. = 136° axis and (c) P.A. = 46° axis directions. The dashed lines at the bottom are the velocity widths, and the solid vertical line at the center is the systemic velocity.

is unknown, and the distances can only be crudely estimated. Due to the small number of proper motions, no distance measurement based on statistical parallax and a model-fitting method was available from our data. Instead, we made "spectrum-like profiles", flux-density profiles against proper motions in the P.A. = 136° axis (direction of the VVCM eigenvector), and in the direction of the respective perpendicular axis P.A. = 46°. In figure 4, (b) represents the velocity profiles projected onto the directions in P.A. = 136°, and (c), that projected onto the P.A. = 46° axis.

The spectrum coverages were 16.3 km s^{-1} in the radial direction, 14.8 km s^{-1} for P.A. = 136° and 10.8 km s^{-1} for P.A. = 46° axis directions at the assumed distance of 170 pc. It is likely that the expanding flow is slightly blocked in the northeast−southwest direction. Thus, when assuming a distance of 170 pc, the spectrum-like profiles indicate that the velocity coverages in the radial and transverse directions are roughly equal. If a distance of 294 pc is

assumed, the velocity coverages on the celestial plane would be double, and would imply an unreliable collimation of the bipolar outflow on the celestial plane. Therefore, a distance of 170 pc is available for R Crt. Note, however, that the maser velocity coverage varies due to a time variation in the maser features.

4. Conclusions

We investigated the 3-D kinematics of water masers around the semi-regular variable star R Crt using data from multi-epoch observations with VLBI at short intervals. It has been verified that most of these maser features existed for at least 80 days. We measured the three-dimensional velocity field, which indicates a possible bipolar outflow. A variance-covariance analysis applied to the velocity field supports the bipolarity of the outflow. The existence of bipolar outflow suggests that a Mira variable had already formed a bipolar outflow. We estimated the inner and outer radii of the water-maser region, which are consistent with those of other observations of R Crt. Water-maser emission in R Crt comes from regions where dust grains are condensed, and where material within the envelope is accelerated until reaching the terminal velocity. It seems that within the water-maser envelopes around R Crt, material is bound to the star in the water-maser regions, and marginally bound outside. We measured the Doppler-velocity drifts of the maser features. The blue-shifted maser features are apparently accelerated, while the red-shifted features are the opposite. If the accelerations of the blue-shifted masers are real, maser features are accelerating toward the terminal velocity. Making spectrum-like profiles from proper motions allowed us to verify the distance of 170 pc to R Crt. Similar observations are encouraged to directly measure the accelerations in CSE to investigate envelopes around stars and to clarify the asymmetric shapes of the CSEs of evolved stars.

We would like to thank an anonymous referee for valuable comments. We would also like to express our gratitude to each member of the Japanese VLBI Network for their support during observations, correlations, and data reduction. H.I. was financially supported by a Japan Society of Promotion of Science fellowship.

References

Bloemhof, E. E. 2000, ApJ, 533, 893

Bowers, P. F. 1992, ApJ, 390, L27

Bowers, P. F., Claussen, M. J., & Johnston, K.J. 1993, AJ, 105, 284

Bowers, P. F., & Johnston, K.J. 1994, ApJS, 92, 189

Bowers, P. F., Johnston, K. J., & de Vegt, C. 1989, ApJ, 340, 479

Chapman, J. M., & Cohen, R. J. 1986, MNRAS, 220, 513

Chikada, Y., Kawaguchi, N., Inoue, M., Morimoto, M., Kobayashi, H., Mattori, S., Nishimura, T., Hirabayashi, H., et al. 1991, in Frontiers of VLBI, ed. H. Hirabayashi, M. Inoue, & H. Kobayashi

(Tokyo: Universal Academy Press), 79
Colomer, F., Reid, M. J., Menten, K. M., & Bujarrabal V. 2000, A&A, 355, 979
Cooke, B., & Elitzur, M. 1985, ApJ, 295, 175
Danchi, W. C., Bester, M., Greenhill, L. J., Degiacomi, C. G., & Townes, C. H. 1994, Proc. SPIE, 2200, 286
Dickinson, D.F., Bechis, K.P., & Barrett, A.H. 1973, ApJ, 180, 831
Engels, D., Kreysa, E., Schultz, G. V., & Sherwood, W. A. 1983, A&A, 124, 123
Gwinn, C. R. 1994, ApJ, 429, 241
Imai, H., Shibata, K. M., Sasao, T., Miyoshi, M., Kameya, O., Omodaka, T., Morimoto, M., Iwata, T., et al. 1997, A&A, 319, L1
Imai, H., Kameya, O., Sasao, T., Miyoshi, M., Deguchi, S., Horiuchi, S., & Asaki, Y. 2000, ApJ, 538, 751
Jewell, P. R., Snyder, L.E., Walmsley, C. M., Wilson, T. L., & Gensheimer, P. D. 1991, A&A, 242, 211
Johnston, K. J., Spencer, J. H., & Bowers, P. F. 1985, ApJ, 290, 660
Kahane, C., & Jura, M. 1994, A&A, 290, 183
Kahane, C., & Jura, M. 1996, A&A, 310, 952
Kawaguchi, N., Kobayashi, H., Miyaji, T., Mikoshiba, H., Tojo, A., Yamamoto, Z., & Hirosawa, H. 1994, in VLBI Technology Progress and Future Observational Possibilities, ed. T. Sasao, S. Manabe, O. Kameya, & M. Inoue (Tokyo: Terra Scientific Publishing Company), 26
Kholopov, P.N., Samus, N. N., Durlevich, O. V., Kazarovets, E. V., Kireeva, N. N., & Tsvetkova, T. M. 1987, General Catalogue of Variable Stars, 4th ed. (Moscow:Nauka)
Knapp, G. R., Young, K., Lee, E., & Jorissen, A. 1998, ApJS, 117, 209
Lane, A. P. 1982, PhD Thesis, Massachusetts University, Amherst
Lane, A. P., Johnston, K. J., Bowers, P.F., Spencer, J. H., & Diamond, P. J. 1987, ApJ, 323, 756
Le Squeren, A. M., Baudry, A., Brillet, J., & Darchy, B. 1979, A&A, 72, 39
Manchado, A., Villaver, E., Stanghellini, L., & Guerrero, M. A. 2000, in ASP Conf. Ser. 199, Asymmetrical Planetary Nebulae II: From Origins to Microstructures, ed. Kastner J. H., Soker N., & Rappaport S. (San Francisco: ASP), 17
Marvel, K. B. 1996, PhD Thesis, New Mexico State University
Omodaka, T., Morimoto, M., Kawaguchi, N., Miyaji, T., Yasuda, S., Suzuyama, T., Kitagawa, T., Miyazaki, T., et al. 1994, in VLBI Technology Progress and Future Observational Possibilities, ed. T. Sasao, S. Manabe, O. Kameya, & M. Inoue (Tokyo: Terra Scientific Publishing Company), 191
Richards, A. M. S., Yates, J. A., & Cohen, R. J. 1996, MNRAS, 282, 665
Richards, A. M. S., Yates, J. A., & Cohen, R. J. 1998, MNRAS, 299, 319
Richards, A. M. S., Yates, J. A., Cohen, R. J. 1999, MNRAS, 306, 954
Sahai, R., Hines, D. C., Kastner, J. H., Weintraub, D. A., Trauger, J. T, Rieke, M. J, Thompson, R. I., & Schneider, G. 1998, ApJ, 492, L163
Szymczak, M., Cohen, R. J., & Richards, A. M. S. 1999, MNRAS, 304, 877
Szymczak, M., & Le Squeren, A. M. 1999, MNRAS, 304, 415
Takaba, H., Ukita, N., Miyaji, T., & Miyoshi, M. 1994, PASJ, 46, 629

Yates, J. A., & Cohen, R. J. 1994. MNRAS, 270, 958
Zuckerman, B., & Dyck, H. M. 1986, ApJ, 304, 394